












Time-frequency component of the GreenX library: minimax grids for efficient RPA and GW calculations

Maryam Azizi ¹, Jan Wilhelm ², Dorothea Golze ³, Matteo Giantomassi ¹, Ramón L. Panadés-Barrueta ³, Francisco A. Delesma ⁴, Alexander Bучcheri ⁵, Andris Gulans ⁶, Patrick Rinke ⁴, Claudia Draxl ⁵, and Xavier Gonze ¹

¹ Institute of Condensed Matter and Nanoscience, UCLouvain, B-1348 Louvain-la-Neuve, Belgium

² Institute of Theoretical Physics and Regensburg Center for Ultrafast Nanoscopy (RUN), University of Regensburg, D-93053 Regensburg, Germany

³ Faculty of Chemistry and Food Chemistry, Technische Universität Dresden, 01062 Dresden, Germany



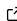
⁴ Department of Applied Physics, Aalto University, P.O. Box 11100, 00076 Aalto, Finland

⁵ Institut für Physik und Iris Adlershof, Humboldt-Universität zu Berlin, Zum Großen Windkanal 2, 12489 Berlin, Germany

⁶ Department of Physics, University of Latvia, Jelgavas iela 3, Riga, LV-1004 Latvia

DOI: [10.21105/joss.05570](https://doi.org/10.21105/joss.05570)

Software

- [Review](#) 
- [Repository](#) 
- [Archive](#) 

Editor: [Lucy Whalley](#)  

Reviewers:

- [@mailhexu](#)
- [@DarioALeonValido](#)

Submitted: 24 May 2023

Published: 27 September 2023

License

Authors of papers retain copyright and release the work under a Creative Commons Attribution 4.0 International License ([CC BY 4.0](#)).

Summary

The central objects in many-body electronic structure theory, such as the *GW* method and the random-phase approximation (RPA), are defined in the complex frequency or time domain. We present here the GX-TimeFrequency component of the GreenX library, providing grids and weights for imaginary time-frequency transformations needed for Green's function based objects. The GreenX library emerged from the NOMAD Center of Excellence, whose objective is to enable accurate Green's function based electronic structure theory calculations on state-of-the-art supercomputers.

The package comprises minimax time and frequency grids ([Kaltak et al., 2014b](#); [Liu et al., 2016](#); [Takatsuka et al., 2008](#)) and corresponding quadrature weights to numerically compute time and frequency integrals of the correlation energy as well as weights for Fourier transforms between time and frequency grids. While targeting low-scaling RPA and *GW* algorithms, its compact frequency grids allows one to reduce the computational prefactor in RPA implementations with conventional scaling. In addition, the time grids can be employed in Laplace-transformed direct MP2 (LT-dMP2) calculations. The GreenX source code is freely available on GitHub, and comes equipped with a build system, a comprehensive set of tests, and detailed documentation.

Statement of need

RPA, an accurate approach to compute the electronic correlation energy, is non-local, includes long-range dispersion interactions and dynamic electronic screening, and is applicable to a wide range of systems from 0 to 3 dimensions ([Eshuis et al., 2012](#); [Ren, Rinke, Joas, et al., 2012](#)). The *GW* method ([Hedin, 1965](#)) is based on the RPA susceptibility and has become the method of choice for the calculation of direct and inverse photoemission spectra of molecules and solids ([Golze et al., 2019](#); [Reining, 2018](#)). Furthermore, *GW* forms the basis for Bethe-Salpeter Equation (BSE) calculations of optical spectra ([Onida et al., 2002](#)).

Despite wide adoption, RPA and *GW* face computational challenges, especially for large systems. Conventional RPA and *GW* implementations scale with the fourth power of system size *N* and are therefore usually limited to systems up to one hundred atoms ([Panadés-Barrueta](#)

& Golze, 2023; Stuke et al., 2020). To tackle larger and more realistic systems, scaling reductions present a promising strategy to decrease the computational cost. Such low-scaling algorithms utilize real-space representations and time-frequency transformations, such as the real-space/imaginary-time approach (Rojas et al., 1995) that reduces the complexity to $\mathcal{O}(N^3)$. Several such cubic-scaling GW algorithms have recently been implemented, e.g. in a plane-wave/projector-augmented-wave GW code (Kutepov et al., 2017; Liu et al., 2016) or with localized basis sets using Gaussian (Duchemin & Blase, 2021; Graml et al., 2023; Wilhelm et al., 2018, 2021) or Slater-type orbitals (Förster et al., 2023; Förster & Visscher, 2020, 2021a, 2021b). Similarly, low-scaling RPA algorithms were implemented with different basis sets (Drontschenko et al., 2022; Duchemin & Blase, 2019; Graf et al., 2018; Kaltak et al., 2014a, 2014b; Shi et al., 2023; Wilhelm et al., 2016).

With larger pre-factor, low-scaling algorithms are typically more expensive for smaller systems and only become more cost-effective than canonical implementations for larger systems thanks to their reduced scaling (Wilhelm et al., 2018). Furthermore, the numerical precision of low-scaling GW algorithms is strongly coupled to the time-frequency treatment (Wilhelm et al., 2021). Early low-scaling GW algorithms did not reach the same precision as canonical implementations (Förster & Visscher, 2020; Vlcek et al., 2017; Wilhelm et al., 2018). Although appropriate Fourier transforms and corresponding time-frequency grids have been implemented (Duchemin & Blase, 2021; Förster & Visscher, 2021a; Liu et al., 2016; Wilhelm et al., 2021), these implementations and grids are tied to particular codes and are often buried deeply inside the code. Furthermore, reuse of such implementations elsewhere is often restricted by license requirements or dependencies on definitions made in the host code.

In this work, we present the GX-TimeFrequency component of the GreenX library, an open-source package distributed under the Apache license (Version 2.0). GX-TimeFrequency provides time and frequency grids and corresponding integration weights to compute correlation energies for Green's function implementations. It also provides Fourier weights to convert between imaginary time and imaginary frequency. The library can be used for low-scaling RPA and GW implementations, or BSE codes, which use (low-scaling) GW as input. The minimax grids are also suitable for RPA implementations with conventional scaling (Del Ben et al., 2015): they are more compact than, e.g., Gauss-Legendre grids, resulting in a reduction of the computational prefactor, while yielding same accuracy (Del Ben et al., 2015). However, minimax grids are not recommended for conventional imaginary-frequency-only GW implementations (Ren, Rinke, Blum, et al., 2012) since they have not been optimized for the frequency integral of the self-energy.

While not being the main target of the library, the minimax time grids can also be utilized to calculate the LT-dMP2 correlation energy (Almlöf, 1991; Glasbrenner et al., 2020; Jung et al., 2004; Kaltak et al., 2014b; Takatsuka et al., 2008). The dMP2 term is one of two terms of the MP2 correlation energy and, in a diagrammatic representation, corresponds to the lowest order of the RPA correlation energy (Ren, Rinke, Joas, et al., 2012). The dMP2 correlation energy can be reformulated using the Laplace transform to obtain the LT-dMP2 expression which scales cubically in contrast to the $\mathcal{O}(N^5)$ scaling of standard MP2.

Mathematical framework

The single-particle Green's function G and the non-interacting susceptibility χ^0 are starting points for several many-body perturbation theory methods. In canonical implementations, $\chi^0(\mathbf{r}, \mathbf{r}', i\omega)$ is often expressed in the Adler-Wiser form (Adler, 1962; Wiser, 1963), where the sums over occupied (index j) and unoccupied (index a) single-particle states ψ are coupled via their corresponding energies ε .

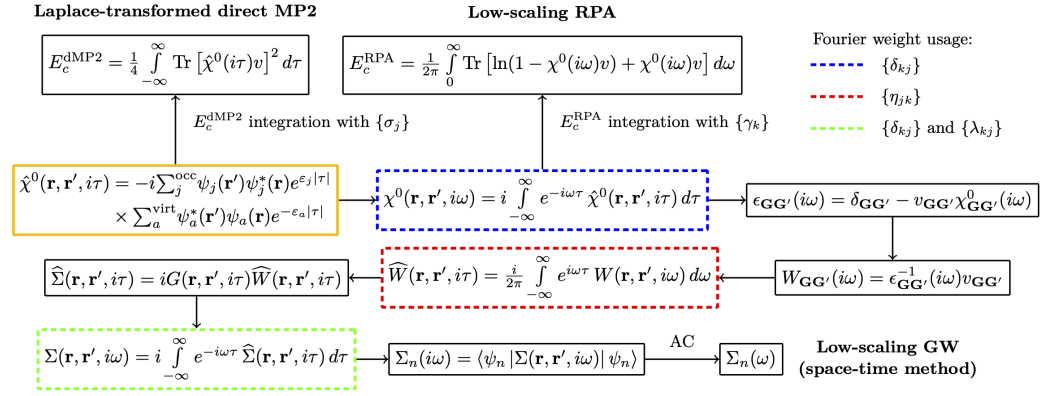


Figure 1: Sketch of the methods supported by GX-TimeFrequency which start from $\hat{\chi}^0(i\tau)$. In addition to the discrete time and frequency grids $\{\tau_j\}$ and $\{\omega_k\}$, the library provides the corresponding weights $\{\sigma_j\}$ and $\{\gamma_k\}$ for the integration of the correlation energy E_c as well as the Fourier weights δ_{kj} , η_{jk} and λ_{kj} defined in Equation 2–Equation 4. The bare and screened Coulomb interactions are indicated by $v(\mathbf{r}, \mathbf{r}') = 1/|\mathbf{r} - \mathbf{r}'|$ and $W(i\omega)$, respectively. $\epsilon(i\omega)$ is the dynamical dielectric function, Σ the GW self-energy, and AC stands for analytic continuation.

The Adler-Wiser expression of $\chi^0(i\omega)$ can be transformed into the imaginary time domain, $\hat{\chi}^0(\mathbf{r}, \mathbf{r}', i\tau) = -iG(\mathbf{r}, \mathbf{r}', i\tau)G(\mathbf{r}', \mathbf{r}, -i\tau)$, yielding the equation in the yellow box in Fig. 1, where the two sums are separated, leading to a favorable $\mathcal{O}(N^3)$ scaling. The polarizability $\hat{\chi}^0(i\tau)$ is the starting point for LT-dMP2 and low-scaling RPA and GW. The low-scaling GW procedure shown in Fig. 1 is known as the space-time method and given here in its original formulation for planewave codes (Rojas et al., 1995).

The time-frequency integrals in Fig. 1 are performed numerically. All three methods in Fig. 1 require a discrete time grid $\{\tau_j\}_{j=1}^n$, where n is the number of grid points. RPA and GW additionally need the discrete frequency grid $\{\omega_k\}_{k=1}^n$. Since $\hat{\chi}^0(\mathbf{r}, \mathbf{r}', i\tau)$ is sharply peaked around the origin and then decays slowly, homogeneous time and frequency grids are inefficient. For this reason, non-uniform grids like Gauss-Legendre (Rieger et al., 1999), modified Gauss-Legendre (Ren, Rinke, Blum, et al., 2012) and the here presented minimax (Kaltak et al., 2014b) grids are used. The minimax grids include also integration weights for the computation of the correlation energies. For the calculation of the LT-dMP2 correlation energy E_c^{dMP2} (Kaltak et al., 2014b; Takatsuka et al., 2008), a time quadrature is performed, for which our library provides the integration weights $\{\sigma_j\}_{j=1}^n$. Similarly, the RPA correlation energy E_c^{RPA} (Del Ben et al., 2015; Kaltak et al., 2014b) is computed from frequency quadrature using integration weights $\{\gamma_k\}_{k=1}^n$.

Low-scaling RPA and GW algorithms include the Fourier transform of $\hat{\chi}^0(i\tau)$ to $\chi^0(i\omega)$ (blue dashed box in Fig. 1). The GW space-time method performs two additional Fourier transforms: The screened Coulomb interaction $W(i\omega)$ is transformed to imaginary time (red dashed box), and the self-energy $\hat{\Sigma}(i\tau)$ is Fourier transformed back to imaginary frequency (green dashed box).

The conversion between imaginary time and frequency grids relies on nonuniform discrete cosine and sine transformations for even and odd functions $F^{\text{even/odd}}$, respectively (Liu et al., 2016). If the function F is neither odd nor even, the computation of functions $\hat{F}(i\tau)$ and $F(i\omega)$ is split into even and an odd parts (Liu et al., 2016)

$$\hat{F}(i\tau) = \hat{F}^{\text{even}}(i\tau) + \hat{F}^{\text{odd}}(i\tau) \quad \text{and} \quad F(i\omega) = F^{\text{even}}(i\omega) + F^{\text{odd}}(i\omega) \quad (1)$$

with $F^{\text{even}}(x) = F^{\text{even}}(-x)$ and $F^{\text{odd}}(x) = -F^{\text{odd}}(-x)$. The same parity rules hold for quantities with a hat. The corresponding discrete Fourier transforms read (Liu et al., 2016)

$$F^{\text{even}}(i\omega_k) = \sum_{j=1}^n \delta_{kj} \cos(\omega_k \tau_j) \hat{F}^{\text{even}}(i\tau_j) \quad (2) \quad F^{\text{odd}}(i\omega_k) = i \sum_{j=1}^n \lambda_{kj} \sin(\omega_k \tau_j) \hat{F}^{\text{odd}}(i\tau_j) \quad (4)$$

$$\hat{F}^{\text{even}}(i\tau_j) = \sum_{k=1}^n \eta_{jk} \cos(\tau_j \omega_k) F^{\text{even}}(i\omega_k) \quad (3) \quad \hat{F}^{\text{odd}}(i\tau_j) = -i \sum_{k=1}^n \zeta_{jk} \sin(\tau_j \omega_k) F^{\text{odd}}(i\omega_k) \quad (5)$$

where $\{\tau_j\}_{j=1}^n, \tau_j > 0$ are again the time grid points, $\{\omega_k\}_{k=1}^n, \omega_k > 0$ frequency grid points and $\{\delta_{kj}\}_{k,j=1}^n, \{\eta_{jk}\}_{k,j=1}^n, \{\lambda_{kj}\}_{k,j=1}^n, \{\zeta_{jk}\}_{k,j=1}^n$ the corresponding Fourier integration weights. $\hat{\chi}^0(i\tau)$ is an even function: the transform defined in Equation 2 yields $\chi^0(i\omega)$. The screened Coulomb interaction is also even and Equation 3 converts $W(i\omega)$ to $\hat{W}(i\tau)$. The self-energy, neither odd nor even, is treated with Equation 1 in combination with Equation 2 and Equation 4 to transform $\hat{\Sigma}(i\tau)$ to $\Sigma(i\omega)$ (Liu et al., 2016). The transformation defined in Equation 5, not required for the methods summarized in Fig. 1, is added for completeness.

Ideal grid parameters $\tau_j, \sigma_j, \omega_k, \gamma_k, \delta_{kj}, \eta_{jk}, \lambda_{kj}$ feature a vanishing error for the LT-dMP2 and RPA correlation energy integrations and Fourier transforms of χ^0, W and Σ (Fig. 1). We compute minimax grid parameters $\tau_j, \sigma_j, \omega_k, \gamma_k$ that minimize the maximum error of the LT-dMP2 and RPA correlation energy integration (Fig. 1) over all possible functions $\hat{\chi}^0(\mathbf{r}, \mathbf{r}', i\tau)$ and $\chi^0(\mathbf{r}, \mathbf{r}', i\omega)$ (Kaltak et al., 2014b; Liu et al., 2016; Takatsuka et al., 2008). This minimax grid optimization relies on the Remez algorithm (Kaltak et al., 2014b), an iterative, numerically ill-conditioned procedure requiring high numerical precision. As the generation of the minimax parameters $\tau_j, \sigma_j, \omega_k, \gamma_k$ is tedious, the computed minimax parameters $\{\tau_j\}_{j=1}^n, \{\sigma_j\}_{j=1}^n, \{\omega_k\}_{k=1}^n, \{\gamma_k\}_{k=1}^n$ are tabulated for their later use in LT-dMP2, RPA, and GW calculations.

It has been shown that minimax time and frequency grids $\{\tau_j\}_{j=1}^n, \{\omega_k\}_{k=1}^n$ are also suitable for performing Fourier transforms of χ^0, W and Σ (Liu et al., 2016). With knowledge of the tabulated $\{\tau_j\}_{j=1}^n$ and $\{\omega_k\}_{k=1}^n$ parameters, least-squares optimization can be used to calculate Fourier integration weights $\delta_{kj}, \eta_{jk}, \lambda_{kj}$. Least-squares optimization can be executed by simple non-iterative linear matrix algebra which is straightforward, and done during the run time of the GreenX library.

The optimal grid parameters $\tau_j, \sigma_j, \omega_k, \gamma_k, \delta_{kj}, \eta_{jk}, \lambda_{kj}$ depend on the energy gap $\min(\varepsilon_a - \varepsilon_j)$ and the maximum eigenvalue difference $\max(\varepsilon_a - \varepsilon_j)$ of the material. We generated minimax grid parameters $\tau_j, \sigma_j, \omega_k, \gamma_k$ assuming energy differences $\varepsilon_a - \varepsilon_j \in [1, R]$, see details in Refs. (Hackbusch, 2019; Kaltak et al., 2014b). Our library stores minimax grid parameters $\{\tau_j(R)\}_{j=1}^n, \{\sigma_j(R)\}_{j=1}^n, \{\omega_k(R)\}_{k=1}^n, \{\gamma_k(R)\}_{k=1}^n$ for $n \in [6, 34]$ and for different values of the range R (on average 15 R -values for each n). For a material with energy gap $\Delta_{\min} := \min(\varepsilon_a - \varepsilon_j)$ and maximum eigenvalue difference $\Delta_{\max} := \max(\varepsilon_a - \varepsilon_j)$, one easily obtains the material-targeted minimax parameters $\{\tau_j^{\text{mat}}\}_{j=1}^n, \{\sigma_j^{\text{mat}}\}_{j=1}^n, \{\omega_k^{\text{mat}}\}_{k=1}^n, \{\gamma_k^{\text{mat}}\}_{k=1}^n$ from rescaling stored parameters with a range $R \geq \Delta_{\max}/\Delta_{\min}$ (Hackbusch, 2019; Kaltak et al., 2014b),

$$\omega_k^{\text{mat}} = \Delta_{\min} \omega_k(R), \quad \gamma_k^{\text{mat}} = \Delta_{\min} \gamma_k(R), \quad \tau_j^{\text{mat}} = \frac{\tau_j(R)}{2\Delta_{\min}}, \quad \sigma_j^{\text{mat}} = \frac{\sigma_j(R)}{2\Delta_{\min}}. \quad (6)$$

Required input and output

GX-TimeFrequency requires as input the grid size n , the minimal eigenvalue difference Δ_{\min} , and the maximal eigenvalue difference Δ_{\max} . For the output parameters, see Table 1. The library component retrieves tabulated minimax parameters $\{\tau_j(R)\}_{j=1}^n, \{\sigma_j(R)\}_{j=1}^n, \{\omega_k(R)\}_{k=1}^n, \{\gamma_k(R)\}_{k=1}^n$ of the requested grid size n for the smallest range R that satisfies $R \geq \Delta_{\max}/\Delta_{\min}$. GX-TimeFrequency then rescales the retrieved minimax parameters according to Equation 6 with Δ_{\min} and prints the results $\{\tau_j^{\text{mat}}\}_{j=1}^n, \{\sigma_j^{\text{mat}}\}_{j=1}^n, \{\omega_k^{\text{mat}}\}_{k=1}^n, \{\gamma_k^{\text{mat}}\}_{k=1}^n$. Fourier integration weights are computed on-the-fly via least-squares optimization. The precision of a global forward cosine transformation followed by backward cosine transformations, is measured from

$$\Delta_{\text{CT}} = \max_{j,j' \in \{1,2,\dots,n\}} \left| \sum_{k=1}^n \eta_{j'k} \cos(\tau_{j'} \omega_k) \cdot \delta_{kj} \cos(\omega_k \tau_j) - (\mathbb{I})_{j'j} \right| \quad (7)$$

with \mathbb{I} being the identity matrix. Inputs and outputs are in atomic units.

Table 1: Output returned by the GX-TimeFrequency component of GreenX. We abbreviate low-scaling as ls, and least-squares optimization as L2 opt.

Output	Description	Methods using the output	Computation
$\{\tau_j^{\text{mat}}\}_{j=1}^n$	time points	LT-dMP2, ls RPA, ls GW	tabulated + rescaling
$\{\sigma_j^{\text{mat}}\}_{j=1}^n$	time integration weights	LT-dMP2	tabulated + rescaling
$\{\omega_k^{\text{mat}}\}_{k=1}^n$	frequency points	ls & canonical RPA, ls GW	tabulated + rescaling
$\{\gamma_k^{\text{mat}}\}_{k=1}^n$	freq. integration weights	ls & canonical RPA	tabulated + rescaling
$\{\delta_{kj}\}_{k,j=1}^n$	Fourier weights	ls RPA, ls GW	on-the-fly L2 opt
$\{\eta_{jk}\}_{k,j=1}^n$	Fourier weights	ls GW	on-the-fly L2 opt
$\{\lambda_{kj}\}_{k,j=1}^n$	Fourier weights	ls GW	on-the-fly L2 opt
Δ_{CT}	duality error	ls GW	on-the-fly

Acknowledgements

Work supported by the European Union's Horizon 2020 research and innovation program under the grant agreement N° 951786 (NOMAD CoE). J.W. and D.G. acknowledge funding by the Deutsche Forschungsgemeinschaft (DFG, German Research Foundation) via the Emmy Noether Programme (Project No. 503985532 and 453275048, respectively). A.G. acknowledges funding provided by the European Regional Development Fund via the Central Finance and Contracting Agency of Republic of Latvia (Project No. 1.1.1.5/21/A/004).

References

- Adler, S. L. (1962). Quantum theory of the dielectric constant in real solids. *Phys. Rev.*, 126(2), 413–420. <https://doi.org/10.1103/PhysRev.126.413>
- Almlöf, J. (1991). Elimination of energy denominators in Møller-Plesset perturbation theory by a Laplace transform approach. *Chem. Phys. Lett.*, 181(4), 319–320. [https://doi.org/10.1016/0009-2614\(91\)80078-C](https://doi.org/10.1016/0009-2614(91)80078-C)
- Del Ben, M., Schütt, O., Wentz, T., Messmer, P., Hutter, J., & VandeVondele, J. (2015). Enabling simulation at the fifth rung of DFT: Large scale RPA calculations with excellent time to solution. *Comput. Phys. Commun.*, 187, 120–129. <https://doi.org/10.1016/j.cpc.2014.10.021>
- Drontschenko, V., Graf, D., Laqua, H., & Ochsenfeld, C. (2022). Efficient Method for the Computation of Frozen-Core Nuclear Gradients within the Random Phase Approximation. *J. Chem. Theory Comput.*, 18(12), 7359–7372. <https://doi.org/10.1021/acs.jctc.2c00774>
- Duchemin, I., & Blase, X. (2019). Separable resolution-of-the-identity with all-electron Gaussian bases: Application to cubic-scaling RPA. *J. Chem. Phys.*, 150(17), 174120. <https://doi.org/10.1063/1.5090605>
- Duchemin, I., & Blase, X. (2021). Cubic-Scaling All-Electron GW Calculations with a Separable Density-Fitting Space-Time Approach. *J. Chem. Theory Comput.*, 17(4), 2383–2393. <https://doi.org/10.1021/acs.jctc.1c00101>
- Eshuis, H., Bates, J. E., & Furche, F. (2012). Electron correlation methods based on the random phase approximation. *Theor. Chem. Acc.*, 131(1), 1084. <https://doi.org/10.1007/s00214-011-1084-8>
- Förster, A., Lenthe, E. van, Spadetto, E., & Visscher, L. (2023). Two-component GW calculations: Cubic scaling implementation and comparison of vertex-corrected and partially

- self-consistent GW variants. *J. Chem. Theory Comput.* <https://doi.org/10.1021/acs.jctc.3c00512>
- Förster, A., & Visscher, L. (2020). Low-order scaling G_0W_0 by pair atomic density fitting. *J. Chem. Theory Comput.*, 16(12), 7381–7399. <https://doi.org/10.1021/acs.jctc.0c00693>
- Förster, A., & Visscher, L. (2021a). GW100: A Slater-Type Orbital Perspective. *J. Chem. Theory Comput.*, 17(8), 5080–5097. <https://doi.org/10.1021/acs.jctc.1c00308>
- Förster, A., & Visscher, L. (2021b). Low-Order Scaling Quasiparticle Self-Consistent GW for Molecules. *Front. Chem.*, 9, 736591. <https://doi.org/10.3389/fchem.2021.736591>
- Glasbrenner, M., Graf, D., & Ochsenfeld, C. (2020). Efficient Reduced-Scaling Second-Order Møller–Plesset Perturbation Theory with Cholesky-Decomposed Densities and an Attenuated Coulomb Metric. *J. Chem. Theory Comput.*, 16(11), 6856–6868. <https://doi.org/10.1021/acs.jctc.0c00600>
- Golze, D., Dvorak, M., & Rinke, P. (2019). The GW compendium: A practical guide to theoretical photoemission spectroscopy. *Front. Chem.*, 7, 377. <https://doi.org/10.3389/fchem.2019.00377>
- Graf, D., Beuerle, M., Schurkus, H. F., Luenser, A., Savasci, G., & Ochsenfeld, C. (2018). Accurate and Efficient Parallel Implementation of an Effective Linear-Scaling Direct Random Phase Approximation Method. *J. Chem. Theory Comput.*, 14(5), 2505–2515. <https://doi.org/10.1021/acs.jctc.8b00177>
- Graml, M., Zollner, K., Hernangómez-Pérez, D., Faria Junior, P. E., & Wilhelm, J. (2023). Low-scaling GW algorithm applied to twisted transition-metal dichalcogenide heterobilayers. *ArXiv e-Prints*. <https://doi.org/10.48550/arXiv.2306.16066>
- Hackbusch, W. (2019). Computation of best L^∞ exponential sums for $1/x$ by Remez' algorithm. *Comput. Vis. Sci.*, 20(1-2), 1–11. <https://doi.org/10.1007/s00791-018-00308-4>
- Hedin, L. (1965). New method for calculating the one-particle Green's function with application to the electron-gas problem. *Phys. Rev.*, 139(3A), A796. <https://doi.org/10.1103/PhysRev.139.A796>
- Jung, Y., Lochan, R. C., Dutoi, A. D., & Head-Gordon, M. (2004). Scaled opposite-spin second order Møller–Plesset correlation energy: An economical electronic structure method. *J. Chem. Phys.*, 121(20), 9793–9802. <https://doi.org/10.1063/1.1809602>
- Kaltak, M., Klimeš, J., & Kresse, G. (2014a). Cubic scaling algorithm for the random phase approximation: Self-interstitials and vacancies in Si. *Phys. Rev. B*, 90(5), 054115. <https://doi.org/10.1103/PhysRevB.90.054115>
- Kaltak, M., Klimeš, J., & Kresse, G. (2014b). Low scaling algorithms for the random phase approximation: Imaginary time and laplace transformations. *J. Chem. Theory Comput.*, 10(6), 2498–2507. <https://doi.org/10.1021/ct5001268>
- Kutepov, A. L., Oudovenko, V. S., & Kotliar, G. (2017). Linearized self-consistent quasiparticle GW method: Application to semiconductors and simple metals. *Comput. Phys. Commun.*, 219, 407–414. <https://doi.org/10.1016/j.cpc.2017.06.012>
- Liu, P., Kaltak, M., Klimeš, J., & Kresse, G. (2016). Cubic scaling GW: Towards fast quasiparticle calculations. *Phys. Rev. B*, 94(16), 165109. <https://doi.org/10.1103/PhysRevB.94.165109>
- Onida, G., Reining, L., & Rubio, A. (2002). Electronic excitations: Density-functional versus many-body green's-function approaches. *Rev. Mod. Phys.*, 74(2), 601. <https://doi.org/10.1103/RevModPhys.74.601>

- Panadés-Barrueta, R. L., & Golze, D. (2023). Accelerating core-level GW calculations by combining the contour deformation approach with the analytic continuation of W. *J. Chem. Theory Comput.*, 19(16), 5450–5464. <https://doi.org/10.1021/acs.jctc.3c00555>
- Reining, L. (2018). The GW approximation: Content, successes and limitations. *Wiley Interdiscip. Rev. Comput. Mol. Sci.*, 8(3), e1344. <https://doi.org/10.1002/wcms.1344>
- Ren, X., Rinke, P., Blum, V., Wieferink, J., Tkatchenko, A., Sanfilippo, A., Reuter, K., & Scheffler, M. (2012). Resolution-of-identity approach to Hartree–Fock, hybrid density functionals, RPA, MP2 and GW with numeric atom-centered orbital basis functions. *New J. Phys.*, 14(5), 053020. <https://doi.org/10.1088/1367-2630/14/5/053020>
- Ren, X., Rinke, P., Joas, C., & Scheffler, M. (2012). Random-phase approximation and its applications in computational chemistry and materials science. *J. Mater. Sci.*, 47(21), 7447–7471. <https://doi.org/10.1007/s10853-012-6570-4>
- Rieger, M. M., Steinbeck, L., White, I., Rojas, H., & Godby, R. (1999). The GW space-time method for the self-energy of large systems. *Comput. Phys. Commun.*, 117(3), 211–228. [https://doi.org/10.1016/S0010-4655\(98\)00174-X](https://doi.org/10.1016/S0010-4655(98)00174-X)
- Rojas, H., Godby, R. W., & Needs, R. (1995). Space-time method for ab initio calculations of self-energies and dielectric response functions of solids. *Phys. Rev. Lett.*, 74(10), 1827. <https://doi.org/10.1103/PhysRevLett.74.1827>
- Shi, R., Lin, P., Zhang, M.-Y., He, L., & Ren, X. (2023). Sub-quadratic scaling real-space random-phase approximation correlation energy calculations for periodic systems with numerical atomic orbitals. *arXiv:2307.12029*. <https://arxiv.org/abs/2307.12029>
- Stuke, A., Kunkel, C., Golze, D., Todorović, M., Margraf, J. T., Reuter, K., Rinke, P., & Oberhofer, H. (2020). Atomic structures and orbital energies of 61,489 crystal-forming organic molecules. *Sci. Data*, 7(1), 1–11. <https://doi.org/10.1038/s41597-020-0385-y>
- Takatsuka, A., Ten-no, S., & Hackbusch, W. (2008). Minimax approximation for the decomposition of energy denominators in Laplace-transformed Møller–Plesset perturbation theories. *J. Chem. Phys.*, 129(4). <https://doi.org/10.1007/s00791-018-00308-4>
- Vlcek, V., Rabani, E., Neuhauser, D., & Baer, R. (2017). Stochastic GW calculations for molecules. *J. Chem. Theory Comput.*, 13(10), 4997–5003. <https://doi.org/10.1021/acs.jctc.7b00770>
- Wilhelm, J., Golze, D., Talirz, L., Hutter, J., & Pignedoli, C. A. (2018). Toward GW calculations on thousands of atoms. *J. Phys. Chem. Lett.*, 9(2), 306–312. <https://doi.org/10.1021/acs.jpcllett.7b02740>
- Wilhelm, J., Seewald, P., Del Ben, M., & Hutter, J. (2016). Large-scale cubic-scaling random phase approximation correlation energy calculations using a Gaussian basis. *J. Chem. Theory Comput.*, 12(12), 5851–5859. <https://doi.org/10.1021/acs.jctc.6b00840>
- Wilhelm, J., Seewald, P., & Golze, D. (2021). Low-scaling GW with benchmark accuracy and application to phosphorene nanosheets. *J. Chem. Theory Comput.*, 17(3), 1662–1677. <https://doi.org/10.1021/acs.jctc.0c01282>
- Wiser, N. (1963). Dielectric constant with local field effects included. *Phys. Rev.*, 129(1), 62–69. <https://doi.org/10.1103/PhysRev.129.62>